Journal of Molecular Graphics and Modelling 35 (2012) 1–10

Contents lists available at SciVerse ScienceDirect

Journal of Molecular Graphics and Modelling

journal homepage: www.elsevier.com/locate/JMGM

Molecular dynamics simulations of the coenzyme induced conformational changes of *Mycobacterium tuberculosis* L-alanine dehydrogenase

Baoping Ling[a], Min Sun[a], Siwei Bi[a], Zhihong Jing[a], Yongjun Liu[b,c,*]

[a] School of Chemistry and Chemical Engineering, Qufu Normal University, Qufu, Shandong 273165, China
[b] Northwest Institute of Plateau Biology, Chinese Academy of Sciences, Xining, Qinghai 810001, China
[c] School of Chemistry and Chemical Engineering, Shandong University, Jinan, Shandong 250100, China

ARTICLE INFO

Article history:
Received 6 October 2011
Received in revised form
31 December 2011
Accepted 26 January 2012
Available online 4 February 2012

Keywords:
L-Alanine dehydrogenase
Mycobacterium tuberculosis
Principle component analysis
Free energy landscape
Molecular dynamics simulations

ABSTRACT

Mycobacterium tuberculosis L-alanine dehydrogenase (L-*Mt*AlaDH) catalyzes the NADH-dependent reversible oxidative deamination of L-alanine to pyruvate and ammonia. L-*Mt*AlaDH has been proposed to be a potential target in the treatment of tuberculosis. Based on the crystal structures of this enzyme, molecular dynamics simulations were performed to investigate the conformational changes of L-*Mt*AlaDH induced by coenzyme NADH. The results show that the presence of NADH in the binding domain restricts the motions and conformational distributions of L-*Mt*AlaDH. There are two loops (residues 94–99 and 238–251) playing important roles for the binding of NADH, while another loop (residues 267–293) is responsible for the binding of substrate. The opening/closing and twisting motions of two domains are closely related to the conformational changes of L-*Mt*AlaDH induced by NADH.

1. Introduction

Tuberculosis infected by *Mycobacterium tuberculosis* poses a serious threat to human health. Annually about 9 million people contract tuberculosis and almost 2 million people die from this disease (http://www.webtb.org/death_rate.php). *M. tuberculosis* has the ability to switch to a dormant or latent phase and persist in the lungs of infected individuals for decades [1]. Currently, the treatment of tuberculosis remains difficult owing to the emergence of multidrug-resistant and extensively drug-resistant strains of *M. tuberculosis*. This provides an enormous potential reservoir for further spread of tuberculosis [2]. Therefore, the development of new antimicrobial drugs for treating this disease is urgently desired.

Although *M. tuberculosis* is able to evade in the immune system and survive in human host for decades in a persistent state [1], when the pathogens were under anaerobic growth conditions or nutrient starvation regimes, one of genes, Rv2780 encoding L-alanine dehydrogenase (L-AlaDH), was found to be up-regulated. Accordingly, the production and activity of this enzyme were observed to increase in *M. tuberculosis* [3,4]. L-AlaDH catalyzes the NADH-dependent reversible oxidative deamination of L-alanine to pyruvate and ammonia [5]. The reversible catalytic mechanism is as follows [6]:

$$\text{l-Alanine} + \text{NAD}^+ + \text{H}_2\text{O} \rightleftharpoons \text{Pyruvate} + \text{NADH} + \text{H}^+ + \text{NH}_4{}^+$$

Earlier kinetic studies from several species have suggested that the catalytic mechanism is predominantly ordered with coenzyme binding. The NADH binds first in the oxidative deamination while the NAD^+ binding occurs first in the reversible reductive amination. However, the binding/releasing order of ammonia and pyruvate varies with different enzymes. L-AlaDH is known to be involved in the generation of pyruvate from alanine during sporulation [7] and required for the normal development of the gram-negative bacterium *Myxococcus xanthus* during vegetative growth and myxospore formation [8].

Structural analysis demonstrates that L-AlaDH shows larger sequence divergence compared with the other aminoacid dehydrogenases, such as leucine dehydrogenase [9] and glutamate dehydrogenase [10]. However, most of L-AlaDHs from several species form hexameric molecules in solution, for instance, *Phormidium lapideum* [11] and *Bacillus subtilis* [12]. The crystal structures of L-AlaDH from *M. tuberculosis* (L-*Mt*AlaDH) show that the enzyme contains two distinct domains, namely a NAD-binding domain (residues 129–308) and a substrate-binding domain (residues 1–128 and 309–371), which are separated by a

* Corresponding author at: Northwest Institute of Plateau Biology, Chinese Academy of Sciences, Xining, Qinghai 810001, China. Tel.: +86 531 883 655 76; fax: +86 531 885 644 64.
E-mail address: yongjunliu_1@sdu.edu.cn (Y. Liu).

1093-3263/$ – see front matter © 2012 Elsevier Inc. All rights reserved.
doi:10.1016/j.jmgm.2012.01.005

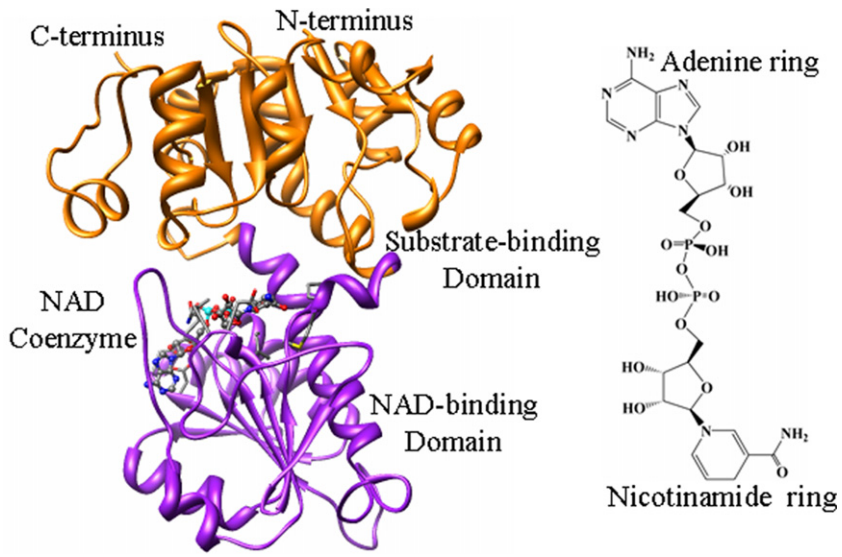

Fig. 1. The X-ray crystal of holo-MtAlaDH (PDB code: 2VOJ, Chain A) and the structure of NADH. The protein is represented by ribbon model with the substrate-binding domain in orange and NAD-binding domain in purple, and the coenzyme NADH is shown in ball and stick model. (For interpretation of the references to color in this figure legend, the reader is referred to the web version of the article.)

cleft, as shown in Fig. 1 [13,14]. The experiments demonstrated that the coenzyme stabilizes the closed structure of the enzyme (holo-*Mt*AlaDH), while the substrate-binding domain rotates by 16° toward the dinucleotide-binding domain compared with its opened structure (apo-*Mt*AlaDH)[13]. So far, the conformational changes of protein upon binding NADH have not been studied in detail, and the motional mode and driving force of the conformational change are still unclear. To investigate the conformational changes of L-*Mt*AlaDH upon coenzyme binding at the atomic level, molecular dynamics simulations were performed since molecular dynamics (MD) simulations have been useful for investigating the conformational changes in proteins [15–18].

2. Methods

2.1. Preparation of models

The X-ray crystal structures of L-*Mt*AlaDH were used for preparing initial structures for MD simulations. The opened structure of enzyme (apo-*Mt*AlaDH) was taken from the Brookhaven Protein Data Bank (PDB code 2VOE with resolution of 2.60 Å), and the closed structure (holo-*Mt*AlaDH) was obtained from the crystal structure refined at 2.60 Å resolution with PDB code 2VOJ [13]. Since the present study focuses on the conformational change of L-*Mt*AlaDH induced by binding coenzyme NADH (NAD), the starting hybrid structure (holo-*Mt*AlaDH-hybrid), namely the enzyme has already complexed with the coenzyme but without the conformational changes, was downloaded from the Brookhaven Protein Data Bank, and PDB code was 2VHW with 2.0 Å resolution [14]. These crystal structures composed of several chains are intact and no missing residues. Table 1 compares chains A–F in three crystal structures in terms of Cα root-mean-square deviation (RMSD), and Fig. S1 of the supporting information gives their chains superposed by an RMSD fit between Cα atoms. Differences between their chains are small enough to be covered by movement of MD simulations even though either chain is selected for MD simulation, accordingly chain A of each crystal structure was chosen to serve as the starting structure. Water molecules within 5 Å surrounding NAD were retained, and the remainder were deleted from the crystal structures [19].

2.2. Parameters setup for molecular dynamics simulations

The respective system was solvated in the simple point charge (SPC) water [20] cubic box with periodic boundary conditions. To neutralize the overall charge of the system, 7, 8 and 8 water molecules were replaced randomly by corresponding Na^+ counter ions in three systems of apo-*Mt*AlaDH, holo-*Mt*AlaDH-hybrid and holo-*Mt*AlaDH. At the end, the apo-*Mt*AlaDH system is composed 75,195 atoms in a 9.2 nm × 9.2 nm × 9.2 nm box, and the holo-*Mt*AlaDH-hybrid system contains 68,507 atoms in 8.9 nm × 8.9 nm × 8.9 nm box and the holo-*Mt*AlaDH system includes 72,299 atoms in 9.1 nm × 9.1 nm × 9.1 nm box [21,22]. The solvent, protein, NADH and Na^+ were separately coupled to a constant temperature of 300 K, and the modified Berendsen thermostat [23] was applied using a relaxation time of 0.1 ps. The pressure was maintained at 1 atm with isotropic scaling and a relaxation time constant 2.0 ps. The LINCS algorithm [24] was applied to constrain all bond lengths including hydrogen atoms. Long-range electrostatic interactions were calculated using the Partial-Mesh-Ewald (PME) method [25]. The parameters of NAD were generated by PROGRG server in GROMOS96 force filed [26], and standard protonation states were assigned by default for all residues in proteins by the pdb2gmx module. All the molecular dynamics simulations were carried out with the software package GROMACS version 4.0.4 [27,28] in GROMOS96 force field [29].

First, each system was energy-minimized for 10,000 steps using a steepest-decent algorithm; subsequently, the solvent, NAD and ions were equilibrated for 100 ps in constant volume (NVT) and constant pressure (NPT) ensembles, respectively, while the heavy atoms of the protein were restrained harmonically using a force constant of 1000 kJ mol^{-1} nm^{-2}. Finally, three systems were performed for 50 ns MD simulations after removing all the restraints, and all the trajectories were stored every 10 ps for further analysis [30].

2.3. Principle component analysis (PCA)

PCA was performed to reveal the concerted motions of domains from the MD trajectories. Its principle has been described in detail elsewhere [31–33]. PCA is based on the calculation of

Table 1
Comparison of six chains in three PDB structures.

PDB code	Chain A	Chain B	Chain C	Chain D	Chain E	Chain F
2VOE	–	0.082	0.113	0.086	0.145	0.089
2VOJ	–		0.083		0.102	
2VHW	–	0.166	0.392	0.327	0.696	0.670

Chains B–F were superposed on chain A in terms of Cα root-mean-square deviation (Å).

diagonalization of the covariance matrix of atomic positional fluctuations, and yields a set of eigenvectors and eigenvalues. Only the eigenvectors with large eigenvalues are important for describing the significant motions of protein. The present work focused on the conformational changes of protein, therefore, PCA was performed on the fluctuations using Cartesian coordinates of C_α atoms [31] around the energy-minimized structures.

The root mean square inner product (RMSIP) [34,35] between the subspaces of different systems is calculated to measure their dynamic similarity. The value of RMSIP is 1 if two sets of eigenvector are identical, while the RMSIP value is 0 if they are completely orthogonal [36,37]. In this study the RMSIP value between the first 10 eigenvectors of two different sets is defined as follows:

$$\mathrm{RMSIP} = \sqrt{\frac{1}{10}\sum_{i=1}^{10}\sum_{j=1}^{10}(\eta_i^a \nu_j^b)^2}$$

where η_i^a and ν_j^b are the ith and jth eigenvectors from the different systems, respectively [36].

3. Results and discussion

Each system was subjected to 50 ns MD simulations, and the results were analyzed to explore the dynamic properties of L-*Mt*AlaDH as well as the conformational changes of L-*Mt*AlaDH induced by NAD. The figures were created by Chimera [38] and VMD [39].

3.1. The stability and flexibility of L-MtAlaDH

The equilibration of the system and the flexibility of protein were studied by using MD simulations. The RMSDs of Cα atoms were calculated for each system, as shown in Fig. 2. For apo-*Mt*AlaDH system (Fig. 2A), the values of RMSD fluctuate at 0.4 nm after 23 ns during the MD simulations. For holo-*Mt*AlaDH-hybrid system (Fig. 2B), the RMSD of protein maintains at 0.4 nm after 15 ns except for a fluctuation at 23 ns, and the RMSD of NAD also fluctuates at 23 ns. While the RMSD of NAD relative to protein fluctuates at 0.5 nm from 5 to 23 ns, but it increases abruptly to 0.8 nm at 23 ns and finally stabilizes at 0.6 nm after 25 ns. By comparing the distances between adenine or nicotinamide ring and the surrounding residues in supporting information (Fig. S2), we can conclude that the fluctuations of RMSD at 23 ns is mainly caused by the instability of adenine ring of NAD, because it suddenly keeps away from Leu249 and approaches to Asn200 at 23 ns, while the nicotinamide ring is always stable for hydrogen bond interactions with the surrounding residues during MD simulations. For holo-*Mt*AlaDH system in Fig. 2C, the RMSD of protein is always maintained at 0.4 nm after 20 ns, but the RMSD of NAD increases from 0.18 to 0.25 nm at 42 ns, which is caused by the movements of adenine ring (see Fig. S2D). The adenine ring is not stable because it weakly interacts with the surrounding residues through hydrophobic contacts. However, the movement of adenine ring of NAD does not influence the conformation of the substrate-binding domain, because the RMSDs in Figs. S2A and S1B are very stable during MD simulations. However, compared with the RMSDs of substrate-binding domain, the RMSDs of NAD-binding domain at lower values display several fluctuations, indicating the structure of NAD-binding domain is not very stable (see Fig. S2A and S2B), which is consistent with the B factors of crystal structures in Fig. 3. These results indicate that the three systems basically reach equilibrium and the structures of proteins are stable after 23 ns during the MD simulations.

The root mean-square fluctuation (RMSF) of each residue is also calculated to assess the convergence of dynamic properties. Fig. 3 gives the RMSF of the residues derived from the MD simulations. For comparison, the atomic B factors from the X-ray crystal structure were transformed to RMSF with the formula $\langle \Delta r_i^2 \rangle = 3B_i/(8\pi^2)$ [40], which are also shown in Fig. 3. It is obvious that the values of RMSF in Fig. 3A are higher than those in Fig. 3B and C, suggesting that the presence of NAD in the binding domain stabilizes the structure of protein and restricts the fluctuations of the residues. In addition, except for C- and N-terminals, the residues with higher

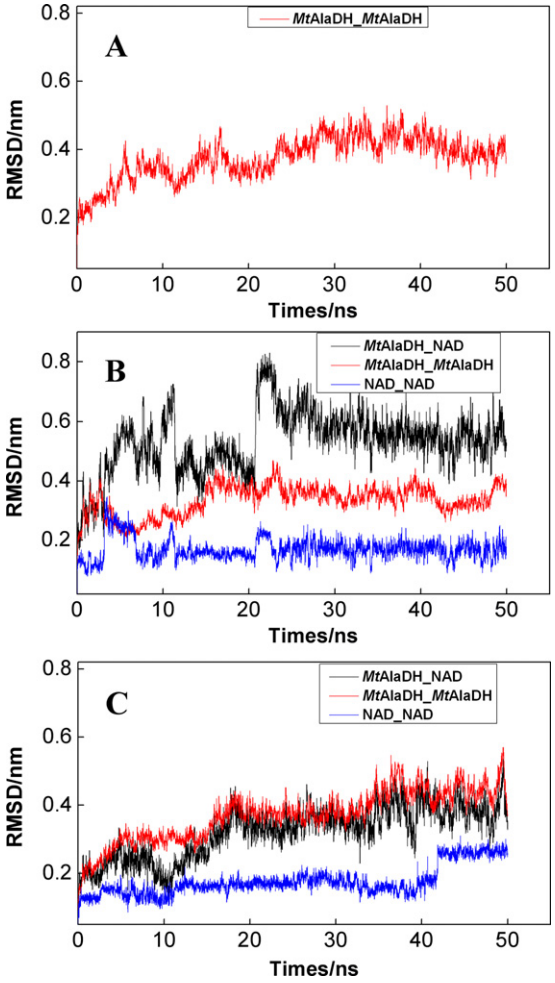

Fig. 2. Time dependence of the RMSDs of L-*Mt*AlaDH with respect to the energy-minimized structure (in red line), L-*Mt*AlaDH with respect to NAD (in black line) and NAD with respect to NAD (in blue line) from the 50 ns MD simulations in three systems. (A) Apo-*Mt*AlaDH system; (B) holo-*Mt*AlaDH-hybrid system; (C) holo-*Mt*AlaDH system. (For interpretation of the references to color in this figure legend, the reader is referred to the web version of the article.)

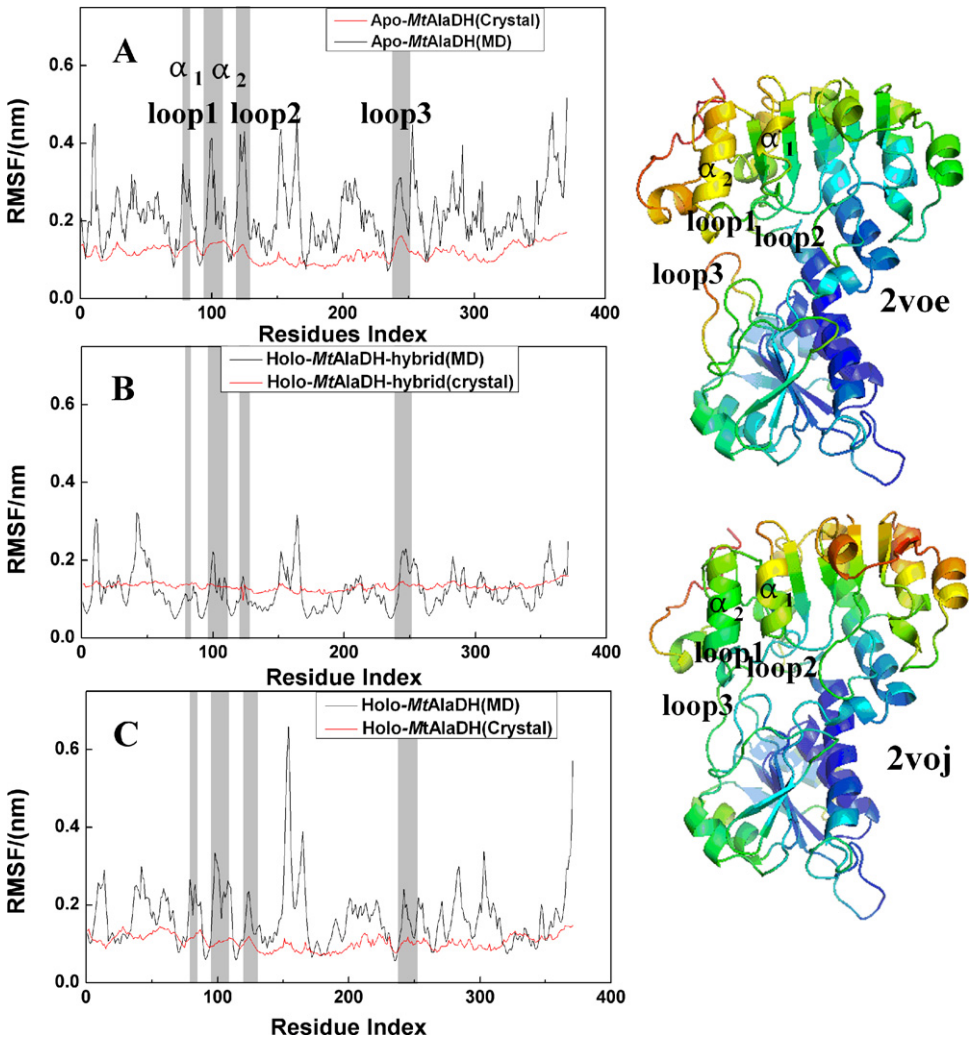

Fig. 3. RMSF of Cα atoms around the energy-minimized structure obtained from MD simulations for three systems. The highly flexible α-helixes and loops neighboring the cleft are highlighted (α1: residues 80–84; α2: residues 100–110; loop1: residues 95–99; loop2: residues 120–126; loop3: residues 238–251). The crystal structures of apo-*Mt*AlaDH (PDB 2voe, Chain A) and holo-*Mt*AlaDH (PDB 2voj, Chain A) are colored by spectrum from blue to red, which represents B factor ranging from 9 to 78. (For interpretation of the references to color in this figure legend, the reader is referred to the web version of the article.)

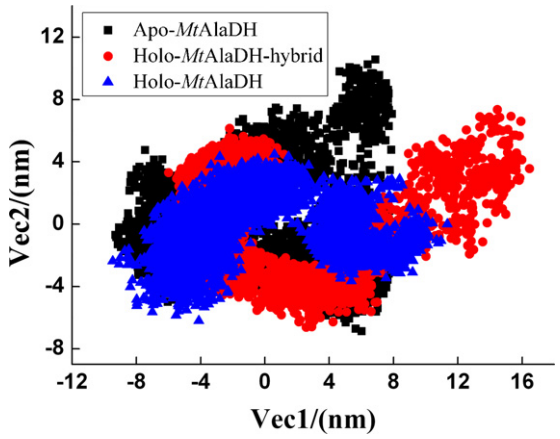

Fig. 4. The 2D projections of Cα trajectories along with the first two eigenvectors derived from molecular dynamics simulations. Apo-*Mt*AlaDH is colored in black, holo-*Mt*AlaDH-hybrid in red and holo-*Mt*AlaDH in blue. (For interpretation of the references to color in this figure legend, the reader is referred to the web version of the article.)

flexibility beside the cleft are two α-helixes (α_1 and α_2) and three loops (loop1, loop2 and loop3), which is in agreement with experiment.

3.2. PCA and domain motions of L-MtAlaDH

In order to determine the concerted conformational motions of protein, PCA was performed to identify the collective motions relevant to protein function [31]. Since the first 10 eigenvalues contributed to the total variance account for 82.8%, 81.7% and 80.7% for apo-*Mt*AlaDH, holo-*Mt*AlaDH-hybrid and holo-*Mt*AlaDH, respectively, the first 10 eigenvectors are used to analyze the protein motions.

The RMSIP was calculated using the first 10 eigenvectors to compare the similarity of protein motions for the three systems. The RMSIP reflects the similarity of motional directions while the trace of covariance matrix describes the strength of motions. The calculated values are listed in Table 2. The RMSIP values between apo-*Mt*AlaDH and holo-*Mt*AlaDH, apo-*Mt*AlaDH and holo-*Mt*AlaDH-hybrid, as well as holo-*Mt*AlaDH-hybrid and holo-*Mt*AlaDH are 0.396, 0.664 and 0.378, respectively. These data suggest that the similarities of motions for the same protein under

Table 2
The calculated RMSIP between of each simulations and the trace of covariance matrix.

Systems	Apo-*Mt*AlaDH	Holo-*Mt*AlaDH-hybrid	Holo-*Mt*AlaDH
Apo_*Mt*AlaDH	–	0.664	0.396
Apo_*Mt*AlaDH_NAD	0.664	–	0.378
Holo_*Mt*AlaDH	0.396	0.378	–
Trace of covariance matrix (nm^2)	52.624	48.153	37.863

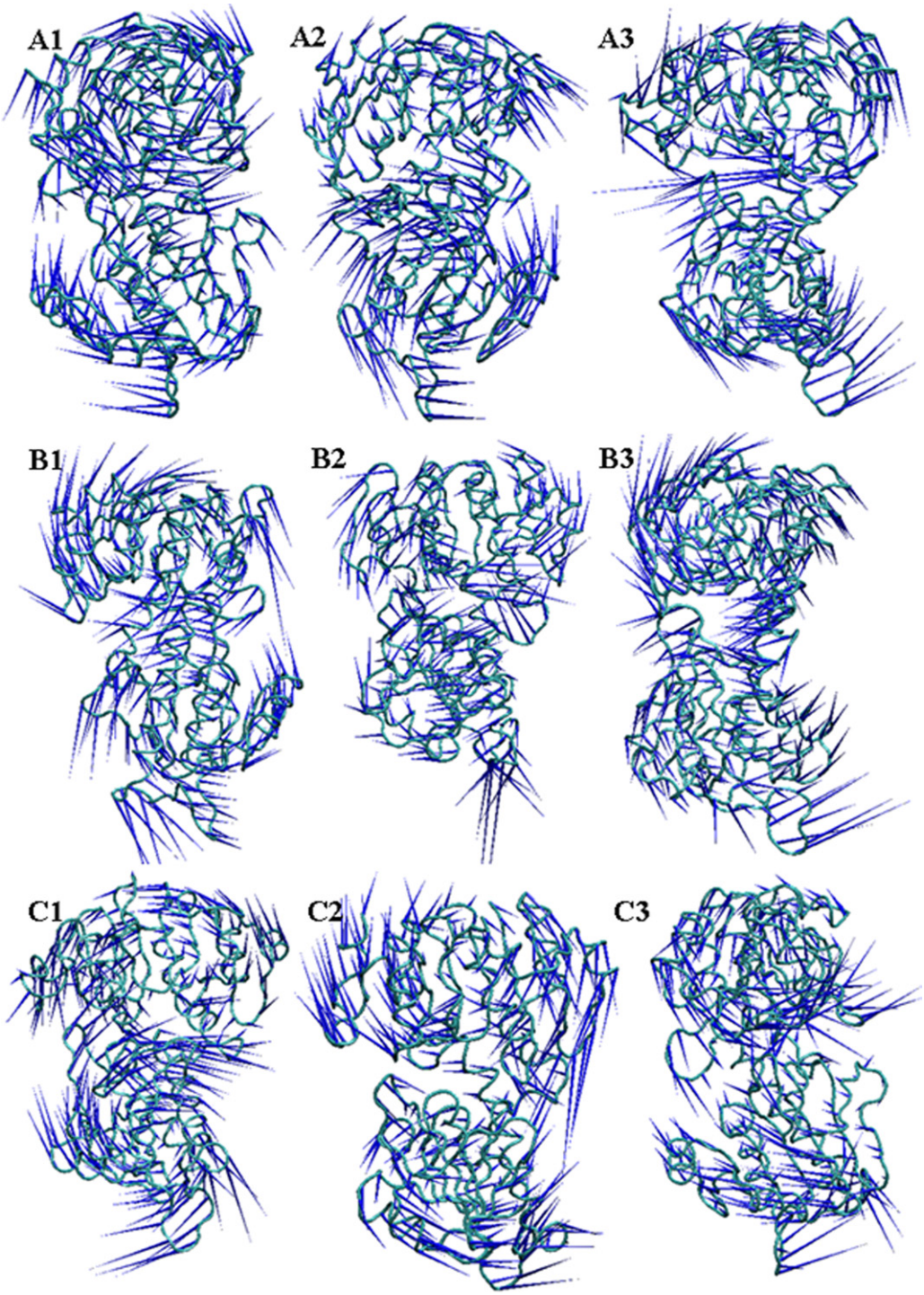

Fig. 5. Porcupine plots of the principle component by using DynDom program. The cone points to the direction that the atom moves in that mode of motion. The amplitude of the motion is represented by the length of the cone. (A1–3), (B1–3) and (C1–3) represent the 1st, 2nd and 3rd eigenvectors of apo-*Mt*AlaDH, holo-*Mt*AlaDH and holo-*Mt*AlaDH-hybrid, respectively. Default DynDom parameters were used.

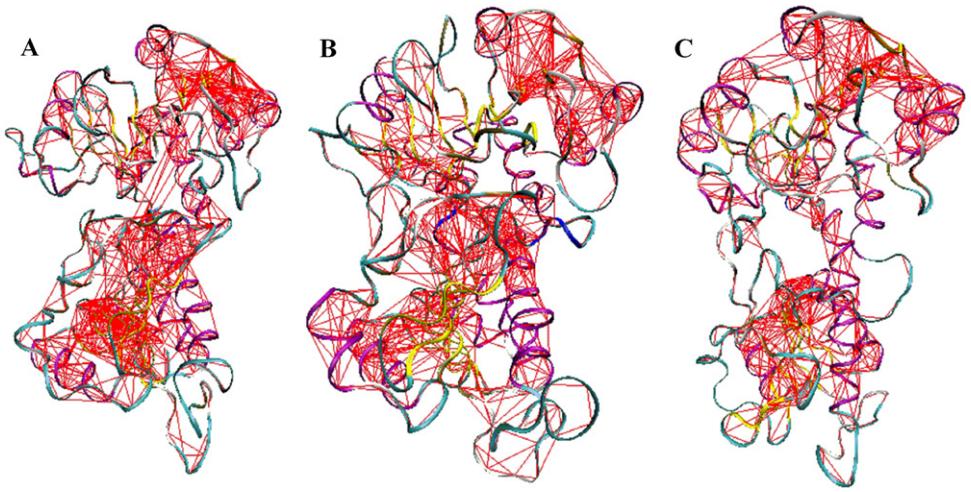

Fig. 6. The covariance web plots of proteins from the three systems. Pairs of atoms with correlation of 0.8 are joined with red lines. The secondary structures are emphasized in different colors, and helix in purple, β-sheet in yellow, turn in cyan. (A) Apo-*Mt*AlaDH, (B) holo-*Mt*AlaDH-hybrid and (C) holo-*Mt*AlaDH. (For interpretation of the references to color in this figure legend, the reader is referred to the web version of the article.)

different conditions are low, and the presence of NAD seriously affects the internal motions of protein. The values of trace of covariance matrix for the three systems are 52.624, 48.153 and 37.863 nm^2, respectively, demonstrating that NAD clearly influences the motional strength of protein, which is supported by the values of RMSF in Fig. 3.

The 2D projections of three trajectories along with the first two eigenvectors are given in Fig. 4. We can see that holo-*Mt*ALaDH shows the smallest conformational space, but holo-*Mt*AlaDH-hybrid shows larger space due to the structural changes of protein upon NAD binding, which reveals that holo-*Mt*AlaDH is the most stable during MD simulations [41]. These results are in agreement with the above RMSIP values, further verifying that the motional direction and strength of protein are restricted by NAD.

The porcupine plots of the principle components are given in Fig. 5, which shows the correlation between the movement of Cα atoms and functionally collective motion [42,43]. Since the first three eigenvectors from MD simulations are the biggest contributors to the overall motions of the proteins (Fig. S3), only the corresponding collective motions of three systems along the first three eigenvectors are shown. Previous studies suggest that for an enzyme with two domains, the main motions of protein are the rotating/twisting and opening/closing motions between two domains in order to facilitate the binding or translocation of substrate and the release of products [44,45]. For apo-*Mt*AlaDH system, the most significant motion in Fig. 5A1 is a biolobal-flexing motion of counter-rotating vortices, i.e., there is a closing motion between the substrate-binding domain and the NAD-binding domain. The concerted motion of the second eigenvector in Fig. 5A2 describes a twisting motion around a "vertical" axis which is a line linking the center of two domains, and the atomic fluctuations of substrate-binding domain is relatively slight. The counter-rotating vortices with opposite direction in Fig. 5A3 also represent the same biolobal-flexing motion of interdomain, but it is an opening motion between two domains. For the holo-*Mt*AlaDH system, the vortices moving in opposition in Fig. 5B1 indicates that the first dominant motion is an opening motion of interdomain, and the third motion in Fig. 5B3 reflects the similar flexing motions of interdomain. However, the porcupine plot in Fig. 5B2 shows that the second dominant motion is a flexing-twisting motion of the two domains. For the holo-*Mt*AlaDH-hybrid system, the first primary motion in Fig. 5C1 corresponds to the twisting mode of interdomain, while the ranked second eigenvector in Fig. 5C2 implies a flexing-twisting motion of two domains, and in Fig. 5C3 the third concerted motion is a closing motion of two domains [46,47]. Taken together, for three systems under different state, the opening/closing and twisting motions are the main motional modes of interdomain for NAD binding and conformational changes.

Fig. 6 gives the covariance web plots of proteins from the three systems in 50 ns MD simulations. Pairs of atoms moving with a correlation threshold of 0.8 are connected with red lines, and rigid domain is determined by the tendency to undergo concerted motion [48]. One can see that the internal motions of the subdomains for apo-*Mt*AlaDH and holo-*Mt*AlaDH-hybrid systems are similar, however, the interactions between the substrate-binding domain and the NAD-binding domain disappear upon binding NAD in holo-*Mt*AlaDH-hybrid system, which is in accordance with that of holo-*Mt*AlaDH. In addition, it can be seen that holo-*Mt*AlaDH is more rigid compared with the other two systems, i.e., the structure of L-*Mt*AlaDH is more stable after binding of NAD.

3.3. Free energy landscape

After evaluation of the motional direction and strength of protein, we attempt an accurate and reliable description of the conformational changes. The free energy landscapes (FELs) [41] were further calculated based on the three principle components, and the two dimensional projections of the principle component 1 vs 2 or 3 for three systems are shown in Fig. 7. The peak in the profile reflects the stability of conformation, and the conformation with higher peak is more stable. It can be seen that the FELs are quite different among the three systems, in particular, their most major states locate in different regions. For apo-*Mt*AlaDH system (Fig. 7A), the plane has four close peaks, and these peaks are relatively remote. Likewise, the plane in Fig. 7B, spanned by the principle components 1 and 3, has four peaks, and three of them have the same height and stability, and the right peak with higher energy corresponds to the more stable conformation. The probability distributions are quite broad, and the conformational space with deep valley is extensive. For holo-*Mt*AlaDH-hybrid system, the planes in Fig. 7C and D span two main energy basins, and the left region is split into two subconformations, but their energies are remarkably different. For holo-*Mt*AlaDH system, two planes in Fig. 7E and F cover two regions, and the left peak with higher energy implies a more stable

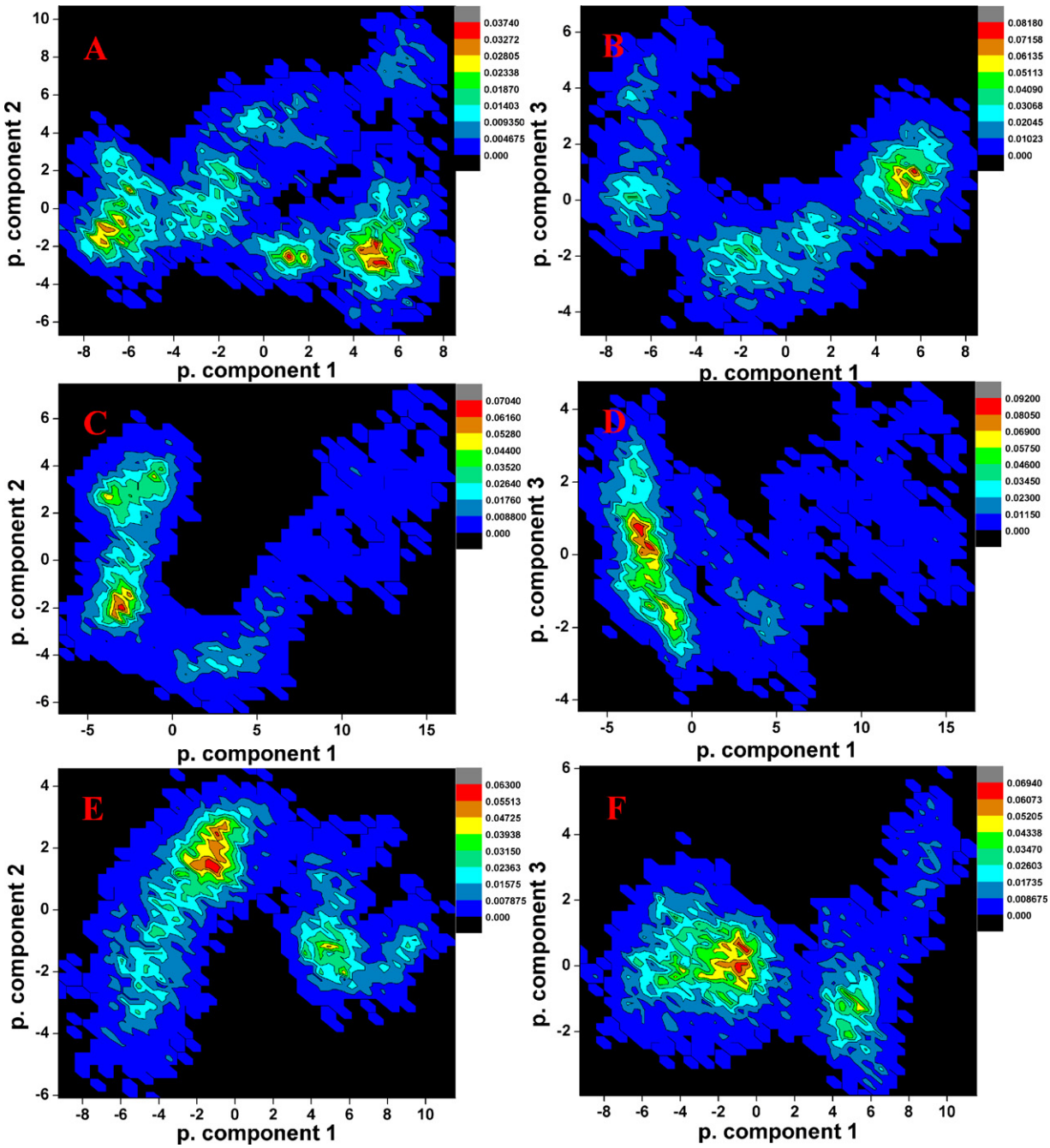

Fig. 7. Free energy landscape projected onto the first three principle components of three systems. On the left hand side, MD trajectories are projected onto the first and second principle component, while on the right hand side, the projections are projected onto the second and third eigenvectors. (A) and (B) for apo-*Mt*AlaDH; (C) and (D) for holo-*Mt*AlaDH-hybrid; (E) and (F) for holo-*Mt*AlaDH. The free energies are represented by $-RT\ln P$, in which P is the distribution probability calculated by the structures sampled at 300 K, and R is the gas constant. The energies are indicated by different colors, and the lowest and highest energies are given in red and black colors, respectively. (For interpretation of the references to color in this figure legend, the reader is referred to the web version of the article.)

conformation. Taken together, the profiles of FEL of holo-*Mt*AlaDH-hybrid are between apo-*Mt*AlaDH and holo-*Mt*AlaDH. However, its major states are more close to those of holo-*Mt*AlaDH. Additionally, the probability distribution of apo-*Mt*AlaDH is broader and the conformational space is more extensive. These results imply that the conformations of protein gradually convert to the closed structure upon binding NAD. Furthermore, the presence of NAD has significant influence on the probability distributions and conformational space of protein.

3.4. Conformational changes of L-MtAlaDH during MD simulations

Fig. 8 gives the superimpositions of average structures of the three systems from MD simulations. These results indicate that the NAD-binding domains overlap well. However, the subtle structural change can be observed within loop3 (residues 238–251), as shown in Fig. 8A and B, and this loop moves about 5 Å to optimize its structure upon binding NAD, which is larger than that of experimental

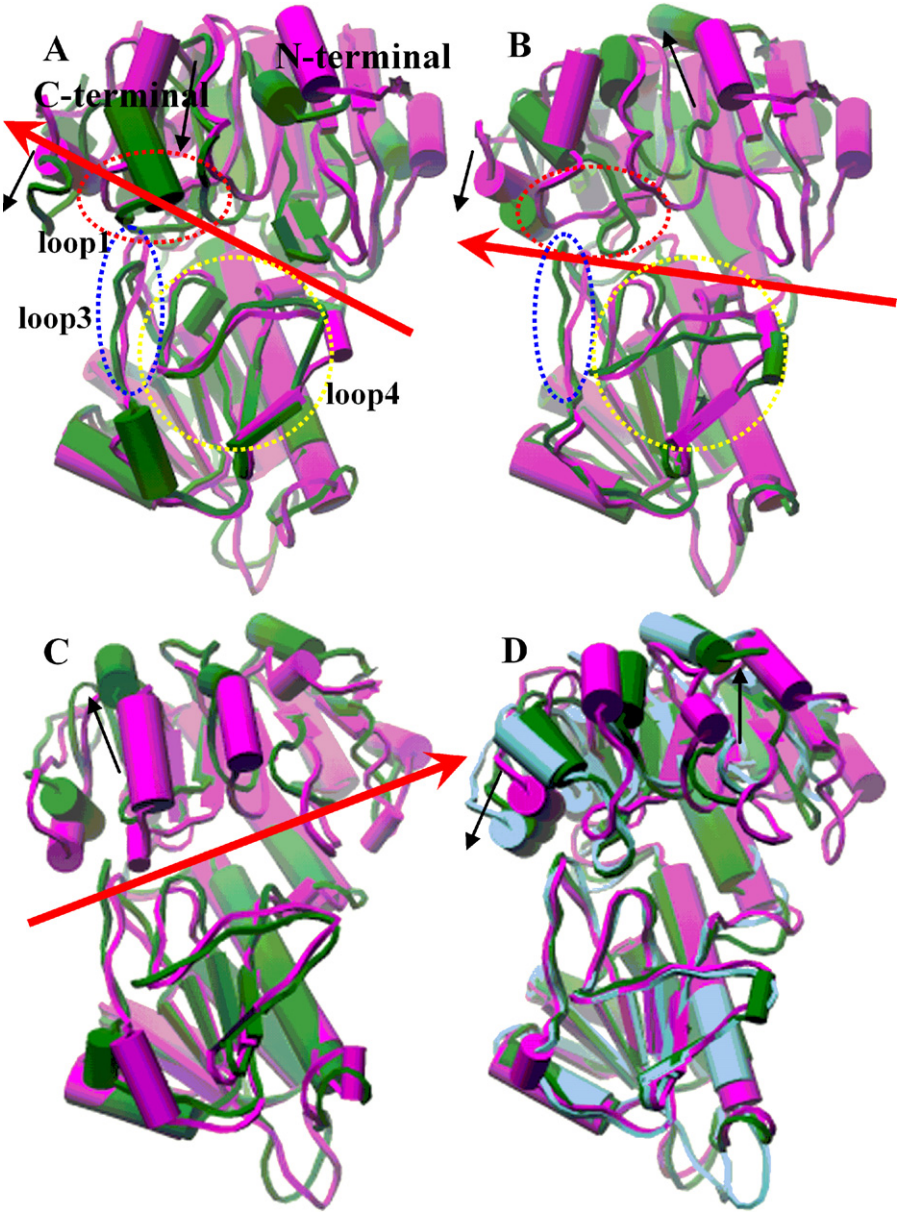

Fig. 8. Superimposition of the average structures from MD simulations. (A) Apo-*Mt*AlaDH (magenta) and holo-*Mt*AlaDH-hybrid (green), (B) apo-*Mt*AlaDH (magenta) and holo-*Mt*AlaDH from 5 to 15 ns MD simulations (green), (C) holo-*Mt*AlaDH crystal structure (magenta) and the average structure from 5 to 15 ns MD simulations (green), (D) the average structure of holo-*Mt*AlaDH from 5 to 15 (magenta), 20 to 35 (green) and 40 to 50 (cyan) ns, respectively. The loop1 (residues 94–99), loop3 (residues 238–251) and loop4 (residues 267–293) are highlighted in the red, blue and yellow dotted lines, respectively. The distances between two loop3 in A and B are about 5 Å. The red axis represents the substrate-binding domain rotates around the arbitrary axis, and the black axis points the orientation of α-helix displacement.

result (2 Å). Meanwhile, loop4 (residues 267–293) displays a minor displacement in the two superimpositions, and the result agrees well with the high fluctuations in Fig. 3. These findings suggest that the two loops (residues 238–251 and 267–293) play a role in NAD binding and make the neighboring residues in NAD-binding domain rearrange their structures.

By comparing Fig. 8A with the average structure of apo-*Mt*AlaDH, we can see that the substrate-binding domain of holo-*Mt*AlaDH-hybrid rotates about 14.2° around an axis toward the NAD-binding domain (determined by the program DynDom [49]), and the result is comparable to the experimental value of 16° [13,14]. While in Fig. 8B, contrasting to the average structure of apo-*Mt*AlaDH, except the α-helix in C-terminal of holo-*Mt*AlaDH tends to close, the other part of the substrate-binding domain tends to keep away from the NAD-binding domain and rotates about 29.9°, indicating that the closed conformation gradually changes to the opened state during the MD simulations. Moreover, for holo-*Mt*AlaDH system, the superimposition (Fig. 8C) of the average structure during 5–15 ns MD simulation with the crystal structure shows that the substrate-binding domain moves to the open direction and rotates 15.4°. In addition, Fig. 8D gives the superimposition of the average structures of holo-*Mt*AlaDH in different time, further indicating that L-*Mt*AlaDH gradually changes the structure from the closed state to open state during MD simulations. And the displacements of α-helix (residues 357–360) in C-terminal of holo-*Mt*AlaDH-hybrid and holo-*Mt*AlaDH systems are all about 7 Å and less than 11 Å of the experimental result, which are probably due to the high flexibility of C-terminal. Meanwhile the obvious difference in the direction is observed in loop1 (residues 95–99), as shown in Fig. 8A and B.

For holo-*Mt*AlaDH-hybrid system, loop1, loop3, loop4 and α-helix are responsible for the binding of NAD and the substrate,

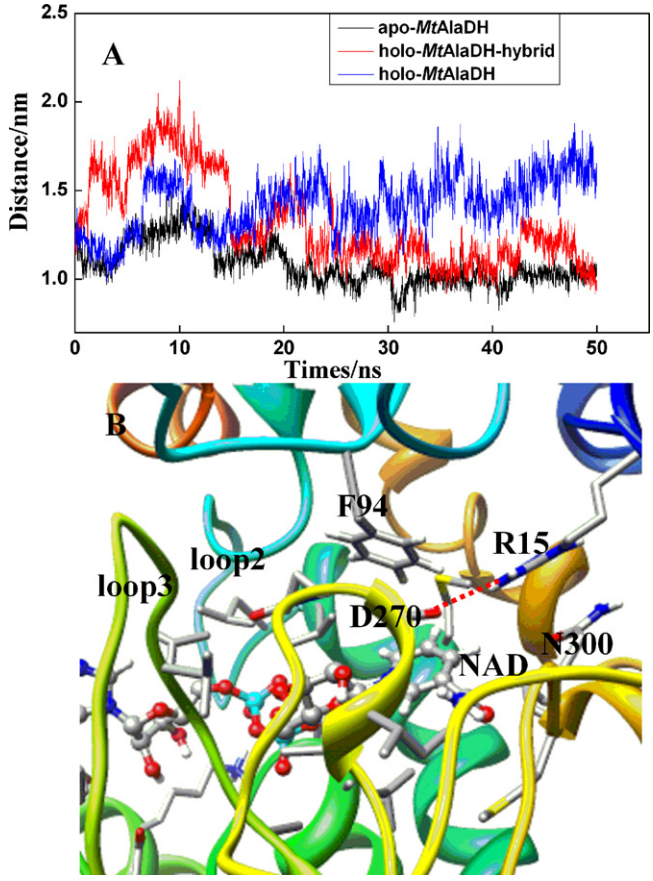

Fig. 9. (A) Time dependence of the distances of mass center between Arg15 in substrate-binding domain and Asp270 in NAD-binding domain for the three systems. (B) NAD (in ball and stick model) and the surrounding residues within 5 Å (in stick model) in the average structure of holo-*Mt*AlaDH-hybrid system. The hydrogen bond is shown in red dashed line. (For interpretation of the references to color in this figure legend, the reader is referred to the web version of the article.)

and lead the substrate-binding domain to rotate toward the NAD-binding domain and form the closed conformation. While for holo-*Mt*AlaDH system, the conformation of protein gradually converts from the closed state to open state during MD simulations.

Fig. 9A shows the time courses of distances of mass center between Arg15 in the substrate-binding domain and Asp270 in the NAD-binding domain during the MD simulations. Although three systems are in different states, the starting distances of two residues are approximately equal. However, they change with the time during the MD simulations. For apo-*Mt*AlaDH and holo-*Mt*AlaDH-hybrid systems, initially, the distances of two residues in different domains gradually increase, then decrease from 10 ns, finally maintain at 1.0 and 1.2 nm after 23 ns, respectively, which further verifies that the conformation of L-*Mt*AlaDH changes from the open state to closed state. However, the distance of two residues for holo-*Mt*AlaDH-hybrid system is always higher than that of apo-*Mt*AlaDH system, especially before 23 ns, which may result from the rearrangement of the neighboring residues of NAD upon binding NAD. The results indicate that the substrate-binding domain was rotated toward NAD-binding domain to facilitate the two residues to form one hydrogen bond to stabilize the closed state (in Fig. 9B). While for holo-*Mt*AlaDH system, the distance decreases gradually before 3 ns, but it increases and fluctuates at 1.6 nm after 3 ns. This result shows that the state of holo-*Mt*AlaDH gradually changes from the closed state to open state, which is in accordance with the superimposition shown in Fig. 8D.

Although the crystal structure shows that water molecules mediate the interactions between NAD and L-*Mt*AlaDH through hydrogen bonds [14], no water molecules are detected in 50 ns MD simulations which perhaps due to the limited timescale.

4. Conclusions

The conformational changes and concerted motions of L-*Mt*AlaDH induced by binding coenzyme have been investigated by means of molecular dynamics simulations. The results show that the conformation of L-*Mt*AlaDH in the systems keeps stable after 23 ns. PCA suggests that the presence of NAD restricts the flexibility and motions of L-*Mt*AlaDH. The open-closing and twisting motions are helpful for the conformational change of L-*Mt*AlaDH. For holo-*Mt*AlaDH-hybrid system, the substrate-binding domain was rotated by 14.2 °C toward the NAD-binding domain. But for holo-*Mt*AlaDH system, the conformation of protein changes from the closed state to open state to facilitate the release of the products. Additionally, loop1 and loop3 play essential roles in NAD binding, and loop4 is important for the substrate binding. These results agree well with the experimental observations [13,14].

In summary, the NAD binding induces the structural rearrangement of residues in active site, meanwhile, the substrate-binding domain moves toward the NAD-binding domain. In other words, the open state converts to the closed state upon binding NAD to facilitate the enzymatic catalysis, while the closed state changes to the open state to assist the releasing of the products.

Acknowledgments

This work was supported by Natural Science Foundation of China (21173129, 21173126) and Shandong Province (ZR2010BM010), and the Scientific Research Startup Funds of Qufu Normal University.

Appendix A. Supplementary data

Supplementary data associated with this article can be found, in the online version, at doi:10.1016/j.jmgm.2012.01.005.

References

[1] L.G. Wayne, L.G. Hayes, An in vitro model for sequential study of shiftdown of *Mycobacterium tuberculosis* through two stages of nonreplicating persistence, Infect. Immun. 64 (1996) 2062–2069.
[2] R. Schnell, G. Schneider, Structural enzymology of sulphur metabolism in *Mycobacterium tuberculosis*, Biochem. Biophys. Res. Commun. 396 (2010) 33–38.
[3] J. Starck, G. Källenius, B. Marklund, D.I. Andersson, T. Åkerlund, Comparative proteome analysis of *Mycobacterium tuberculosis* grown under aerobic and anaerobic conditions, Microbiology 150 (2004) 3821–3829.
[4] S.M. Tripathi, R. Ramachandran, Overexpression, purification, crystallization and preliminary X-ray analysis of Rv2780 from *Mycobacterium tuberculosis* H37Rv, Acta Crystallogr. Sect. F: Struct. Biol. Cryst. Commun. 64 (2008) 367–370.
[5] Å.B. Andersen, P. Andersen, L. Ljungqvist, Structure and function of a 40,000-molecular-weight protein antigen of *Mycobacterium tuberculosis*, Infect. Immun. 60 (1992) 2317–2323.
[6] C.E. Grimshaw, W.W. Cleland, Kinetic mechanism of *Bacillus subtilis* L-alanine dehydrogenase, Biochemistry 20 (1981) 5650–5655.
[7] K.J. Siranosian, K. Ireton, A.D. Grossman, Alanine dehydrogenase (*ald*) is required for normal sporulation in *Bacillus subtilis*, J. Bacteriol. 175 (1993) 6789–6796.
[8] M.J. Ward, H. Lew, D.R. Zusman, Disruption of aldA influences the developmental process in *Myxococcus xanthus*, J. Bacteriol. 182 (2000) 546–550.
[9] P.J. Baker, A.P. Turnbull, S.E. Sedelnikova, T.J. Stillman, D.W. Rice, A role for quaternary structure in the substrate specificity of leucine dehydrogenase, Structure 3 (1995) 693–705.
[10] T.J. Stillman, P.J. Baker, K.L. Britton, D.W. Rice, Conformational flexibility in glutamate dehydrogenase: role of water in substrate recognition and catalysis, J. Mol. Biol. 234 (1993) 1131–1139.

[11] P.J. Baker, Y. Sawa, H. Shibata, S.E. Sedelnikova, D.W. Rice, Analysis of the structure and substrate binding of *Phormidium lapideum* alanine dehydrogenase, Nat. Struct. Biol. 5 (1998) 561–567.
[12] A. Yoshida, E. Freese, Purification and chemical characterization of alanine dehydrogenase from *Bacillus subtilis*, Biochem. Biophys. Acta 92 (1964) 33–43.
[13] D. Ågren, M. Stehr, C.L. Berthold, S. Kapoor, W. Oehlmann, M. Singh, G. Schneider, Three-dimensional structures of Apo- and holo-L-alanine-dehydrogenase from *Mycobacterium tuberculosis* reveal conformational changes upon binding coenzyme binding, J. Mol. Biol. 377 (2008) 1161–1173.
[14] S.M. Tripathi, R. Ramachandran, Crystal structure of the *Mycobacterium tuberculosis* secretory antigen alanine dehydrogenase (Rv2780) in apo and ternary complex forms captures open and closed enzyme conformations, Proteins 72 (2008) 1089–1095.
[15] J.L. Klepeis, K. Lindorff-Larsen, R.O. Dror, D.E. Shaw, Long-timescale molecular dynamics simulations of protein structure and function, Curr. Opin. Struct. Biol. 19 (2009) 120–127.
[16] S.O. Nielsen, R.E. Bulo, P.B. Moore, B. Ensing, Recent progress in adaptive multiscale molecular dynamics simulations of soft matter, Phys. Chem. Chem. Phys. 12 (2010) 12401–12414.
[17] S.O. Nielsen, P.B. Moore, B. Ensing, Adaptive multiscale molecular dynamics of macromolecular fluids, Phys. Rev. Lett. 105 (2010) e237802.
[18] M. Karplus, J.A. McCammon, Molecular dynamics simulations of biomolecules, Nat. Struct. Biol. 9 (2002) 646–652.
[19] H. Fukunishi, H. Yagi, K. Kamijo, J. Shimada, Role of a mutated residue at the entrance of the substrate access channel in cytochrome P450 engineered for vitamin D_3 hydroxylation activity, Biochemistry 50 (2011) 8302–8310.
[20] H.J.C. Berendsen, J.P.M. Postma, W.F. van Gunsteren, J. Hermans, Interaction Models for Water in Relation to Protein Hydration, Reidel, Dordrecht, 1981, pp. 331–342.
[21] J. Zhang, Y. Xu, J. Shen, X. Luo, J. Chen, K. Chen, W. Zhu, H. Jiang, Dynamics mechanism for the autophosphorylation of CheA histidine kinase: molecular dynamics simulations, J. Am. Chem. Soc. 127 (2005) 11709–11719.
[22] S. Hayward, A. Kitao, Molecular dynamics simulations of NAD^+-induced domain closure in horse liver alcohol dehydrogenase, Biophys. J. 91 (2006) 1823–1831.
[23] H.J.C. Berendsen, J.P.M. Postma, W.F. van Gusteren, A. DiNola, J.R. Haak, Molecular dynamics with coupling to an external bath, J. Chem. Phys. 81 (1984) 3684–3690.
[24] B. Hess, H. Bekker, H.J.C. Berendsen, J.E.M. Fraahje, LINCS: a linear constraint solver for molecular interactions, J. Comput. Chem. 18 (1997) 1463–1472.
[25] T. Darden, D. York, L. Pedersen, Particle mesh Ewald. An $N\log(N)$ method for Ewald sums in large systems, J. Chem. Phys. 98 (1993) 10089–10092.
[26] A.W. Schüttelkopf, D.M.F. van Aalten, PRODRG—a tool for high-throughput crystallography of protein–ligand complexes, Acta Crystallogr. D60 (2004) 1355–1363.
[27] D. van der Spoel, E. Lindahl, B. Hess, A.R. van Buuren, E. Apol, P.J. Meulenhoff, D.P. Tieleman, A.L.T.M. Sijbers, K.A. Feenstra, R. van Drunen, H.J.C. Berendsen, Gromacs User Manual Version 4.0, 2005, www.gromacs.org/.
[28] D. van der Spoel, E. Lindahl, B. Hess, G. Groenhof, A.E. Mark, H.J.C. Berendsen, GROMACS: fast, flexible and free, J. Comput. Chem. 26 (2005) 1701–1718.
[29] C. Oostenbrink, A. Villa, A.E. Mark, W.F. van Gunsteren, A biomolecular force field based on the free enthalpy of hydration and solvation: the GROMOS force-field parameter sets 53A5 and 53A6, J. Comput. Chem. 25 (2004) 1657–1676.
[30] L. Saíz-Urra, M.A. Cabrera, M. Froeyen, Exploring the conformational changes of the ATP binding site of gyrase B from *Escherichia coli* complexed with different established inhibitors by using molecular dynamics simulation, J. Mol. Graph. Model. 29 (2011) 726–739.
[31] A. Amadei, A.B.M. Linssen, H.J.C. Berendsen, Essential dynamics of proteins, Proteins 17 (1993) 412–425.
[32] D.M.F. van Aalten, A. Amadei, A.B.M. Linssen, V.G.H. Eijsink, G. Vriend, H.J.C. Berendsen, The essential dynamics of thermolysin: conformation of the hinge-bending motion and comparison of simulations in vacuum and water, Proteins 22 (1995) 45–54.
[33] D.M.F. van Aalten, J.B.C. Findlay, A. Amadei, H.J.C. Berendsen, Essential dynamics of the cellular retinol-binding protein evidence for ligand-induced conformational changes, Protein Eng. 8 (1995) 1129–1136.
[34] D.M.F. van Aalten, A. Amadei, R. Bywater, J.B.C. Findlay, H.J.C. Berendsen, C. Sander, P.F.W. Stouten, A comparison of structural and dynamic properties of different simulation methods applied to SH3, Biophys. J. 70 (1996) 684–692.
[35] A. Amadei, M.A. Ceruso, A. Di Nola, On the convergence of the conformational coordinates basis set obtained by the essential dynamics analysis of proteins' molecular dynamics simulations, Proteins 36 (1999) 419–424.
[36] X. Zhao, S. Wang, X.F. Gao, X.R. Huang, C.C. Sun, Molecular dynamics simulations investigation of neocarzinostatin chromophore-releasing pathways from the holo-NCS protein, J. Struct. Biol. 169 (2010) 14–24.
[37] Y. Wang, X. Zhao, H. Yu, X. Huang, Releasing of the chromophore from the drug delivery protein C-1027: a molecular dynamics simulations study, J. Struct. Biol. 172 (2010) 284–293.
[38] E.F. Pettersen, T.D. Goddard, C.C. Huang, G.S. Couch, D.M. Greenblatt, E.C. Meng, T.E. Ferrin, UCSF chimera—a visualization system for exploratory research and analysis, J. Comput. Chem. 25 (2004) 1605–1612.
[39] W. Humphrey, A. Dalke, K. Schulten, VMD: visual molecular dynamics, J. Mol. Graph. 14 (1996) 33–38.
[40] S.T. Wlodek, T.W. Clark, R. Scott, J.A. McCammon, Molecular dynamics of acetylcholinesterase dimmer complexed with tacrine, J. Am. Chem. Soc. 119 (1997) 9513–9522.
[41] E. Papaleo, P. Mereghetti, P. Fantucci, R. Grandori, L. De Gioia, Free-energy landscape, principle component analysis, and structural clustering to identify representative conformations from molecular dynamics simulations: the myoglobin case, J. Mol. Graph. Model. 27 (2009) 889–899.
[42] K. Tai, T. Shen, R.H. Henchman, Y. Bourme, P. Marchot, J. Andrew McCammon, Mechanism of acetylcholinesterase inhibition by fasciculin: a 5-ns molecular dynamics simulation, J. Am. Chem. Soc. 124 (2002) 6153–6161.
[43] C.P. Barrett, B.A. Hall, M.E.M. Noble, Dynamite: a simple way to gain insight into protein motions, Acta Crystallogr. D: Biol. Cryst. 60 (2004) 2280–2287.
[44] D.J. Rigden, J.E. Littlejohn, H.V. Joshi, B.L. de Groot, M.J. Jedrzejas, Alternative structural conformations of *Streptococcus pneumoniae* Hyaluronan lyase: insights into enzyme flexibility and underlying molecular mechanism of action, J. Mol. Biol. 358 (2006) 1165–1178.
[45] B.L. de Groot, S. Hayward, D.M.F. van Aalten, A. Amadei, H.J.C. Berendsen, Domain motions in bacteriophage T4 lysozyme: a comparison between molecular dynamics and crystallographic data, Proteins 31 (1998) 116–127.
[46] H.V. Joshi, M.J. Jedrzejas, B.L. de Groot, Domain motions of hyaluronan lyase underlying processive hyaluronan translocation, Proteins 76 (2009) 30–46.
[47] M. Liu, J.G. Su, R. Kong, T.G. Sun, J.J. Tan, W.Z. Chen, C.X. Wang, Molecular dynamics simulations of the bacterial periplasmic heme binding proteins ShuT and PhuT, Biophys. Chem. 138 (2008) 42–49.
[48] C.P. Barrett, M.E.M. Noble, Molecular motions of human Cyclin-dependent kinase 2, J. Biol. Chem. 280 (2005) 13993–14005.
[49] G. Poornam, A. Matsumoto, H. Ishida, S. Hayward, A method for the analysis of domain movements in large biomolecular complexes, Proteins 76 (2009) 201–221.